Supplementary Figures

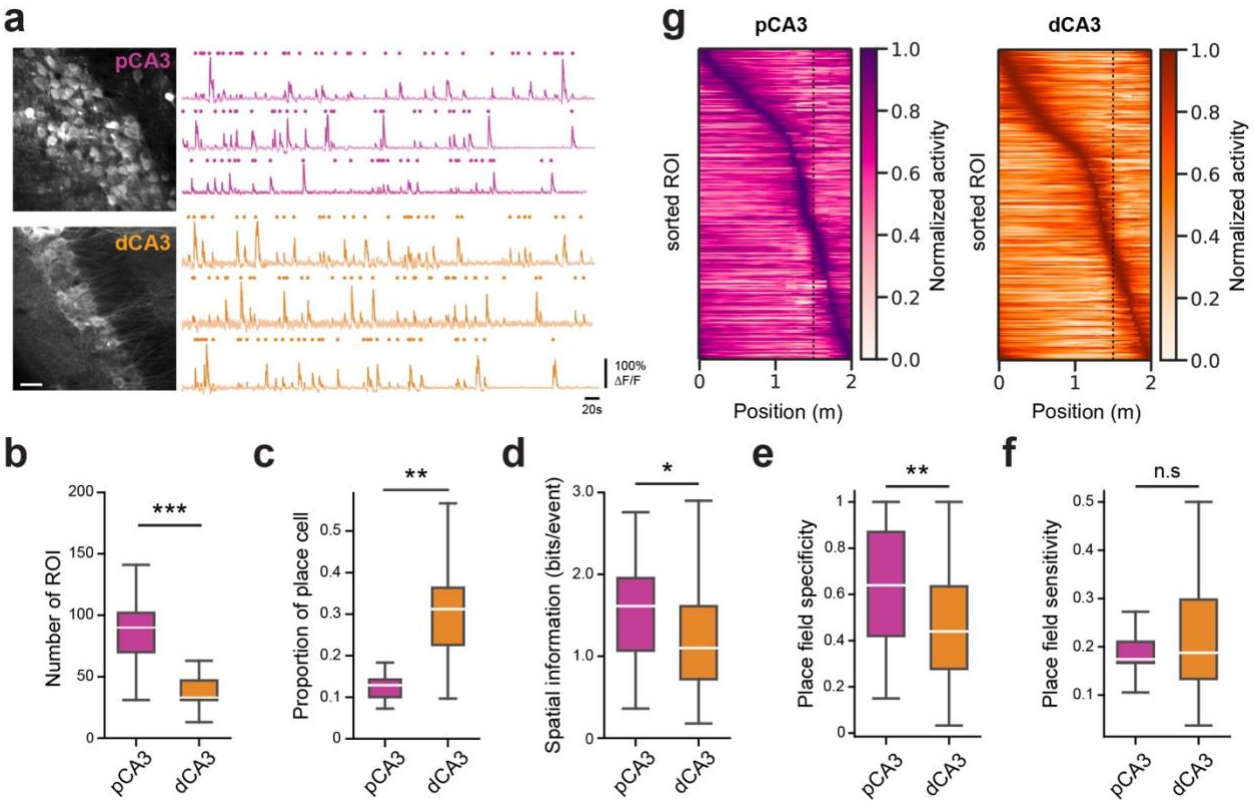

Supplementary Figure 1. (Related to Figure 1) **Spatial tuning of proximal and distal CA3 during spatial navigation. a**. Representative time average image (*left*) and ΔF/F traces (*right*) of proximal (*top*) and distal (*bottom*) CA3 neurons. Transient events in bold and start times indicated by circles above traces. **b**. Average number of detected ROI in proximal and distal CA3 ($p = 3.25 e-5$). **c**. Proportion of place cells in each CA3 subregion (mean ± SEM; $p = 0.0025$; n = 5 and 7 mice for pCA3 and dCA3, respectively). **d**. Spatial information (bits/event) of place cells in each subregion ($p = 0.037$) **e.** Place field specificity in each subregion ($p = 0.0076$). **f**. Place field sensitivity in each subregion ($p = 0.58$). **g**. Heatmaps of spatial tuning curves for pCA3 (*left*) and dCA3 (*right*) cells. Rows show average and normalized responses for all cells, sorted by the position of the peak activity. Mann-Whitney U tests were used to determine statistical significance unless otherwise stated. Colors are matched with purple for pCA3 and orange for dCA3. n.s. = non-significant, *$p < 0.05$, **$p < 0.01$, ***$p < 0.001$.

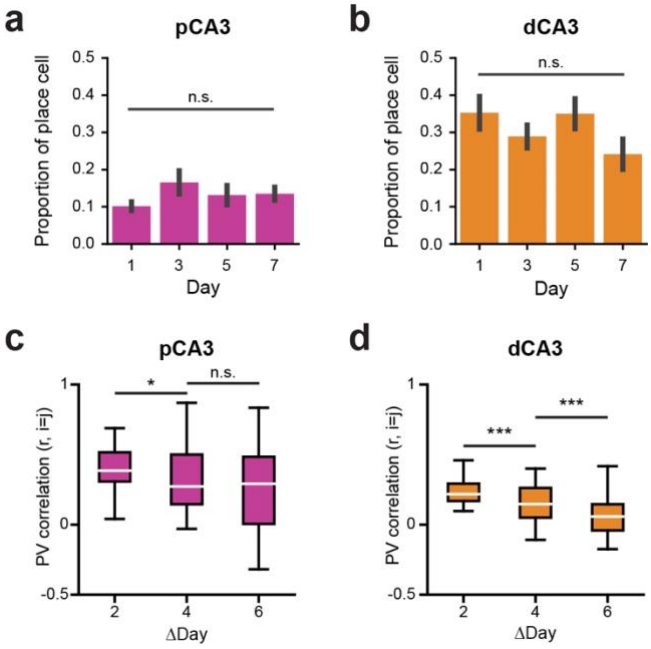

Supplementary Figure 2. (Related to Figure 1) **Long-term stability of place cells in proximodistal CA3. a-b**. Proportion of place cells across days in pCA3 (**a**) and dCA3 (**b**). No significant difference was observed across days in either region (Kruskal-Wallis *H*-test, pCA3: H = 2.69, p = 0.91; dCA3: H = 2.70, p = 0.72; post-hoc Dunn's multiple comparison with Bonferroni correction). **c**-**d**. PV correlation between the same position across days of place cells from pCA3 (**c**) and dCA3 (**d**). Correlation values decreased as interval between days increased. (**c**) p = 0.015 between intervals 2 and 4, p= 0.088 between intervals 4 and 6. (**d**) p = 6.81 e-06 between intervals 2 and 4, p = 0.00014 between intervals 4 and 6. Two-sided unpaired t-tests were used to determine statistical significance. Colors are matched with purple for pCA3 and orange for dCA3. n.s. = non-significant, *p < 0.05, **p < 0.01, ***p < 0.001.

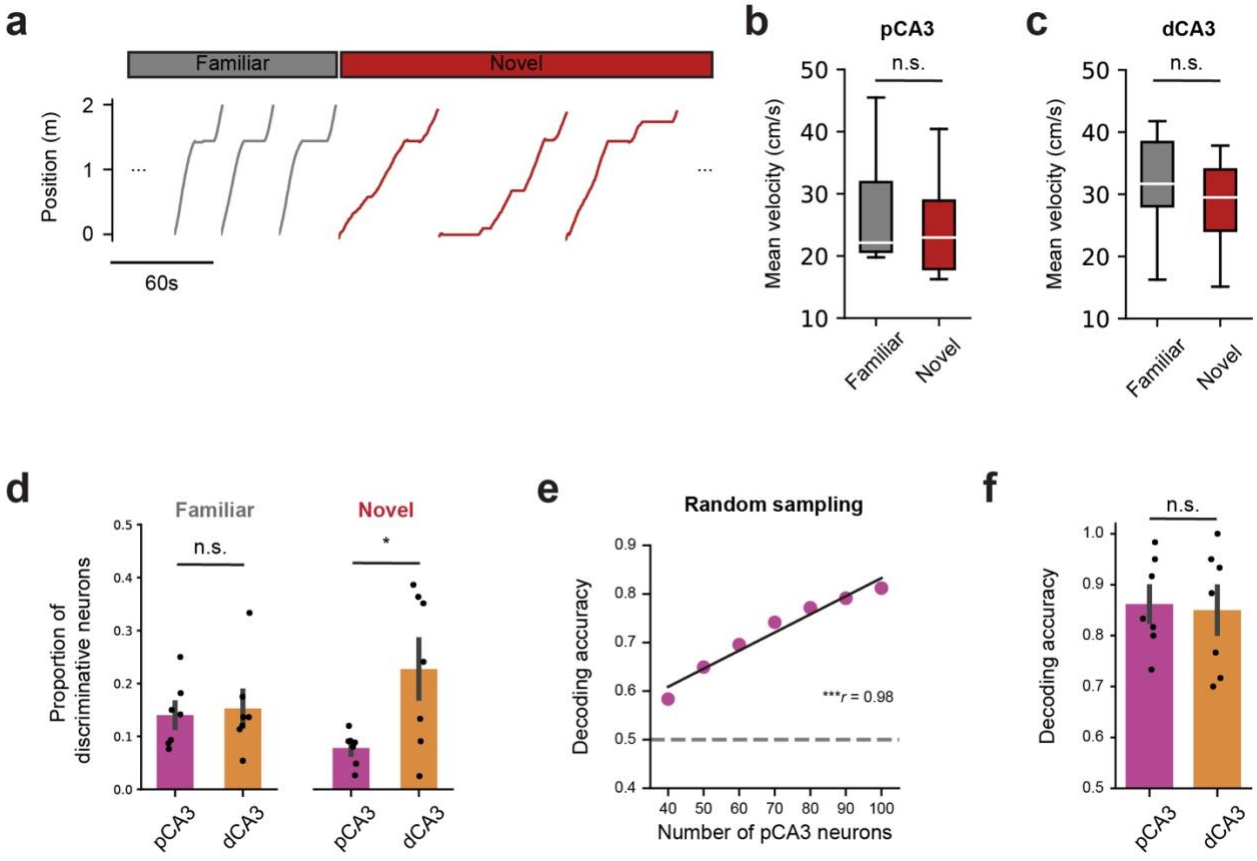

Supplementary Figure 3. (Related to Figure 2) **Context-discriminative neural activity in proximodistal CA3. a**. Position of the animal in the familiar and novel environments from an example session. **b-c**. Comparison of mean velocity in the familiar and novel environments for pCA3 (b) ($p = 0.53$; n = 7mice) and dCA3 (c) ($p = 0.32$; n = 7mice) recording sessions. **d**. Proportion of neurons with significant DI value in familiar and novel environments (7 mice for both pCA3 and dCA3). The proportion of PNs significantly tuned to the familiar environment was similar between pCA3 and dCA3 (0.14 ± 0.23 for pCA3, 0.15 ± 0.03 for dCA3; $p = 1.0$), but dCA3 showed a higher level of novelty-tuned neural responses compared to pCA3 (0.078 ± 0.012 for pCA3, 0.23 ± 0.055 for dCA3; $p = 0.021$). **e**. Peak decoding accuracy correlated with the number of randomly subsampled pCA3 neurons (Pearson's $r = 0.98$, $p = 0.00015$, 7 mice). The black line indicates the regression line. **f**. Performance of the linear decoder for context in pCA3 and dCA3 without subsampling. No significant differences were found in peak decoding accuracies between pCA3 and dCA3 (0.86 ± 0.034 for pCA3, 0.85 ± 0.046 for dCA3, $p = 0.85$, 7 mice for both pCA3 and dCA3). Mann-Whitney U tests were used to determine statistical significance unless otherwise stated. Colors are matched as follows: purple for pCA3, orange for dCA3, gray for familiar context, and red for novel context. n.s. = non-significant, *$p < 0.05$, **$p < 0.01$, ***$p < 0.001$.

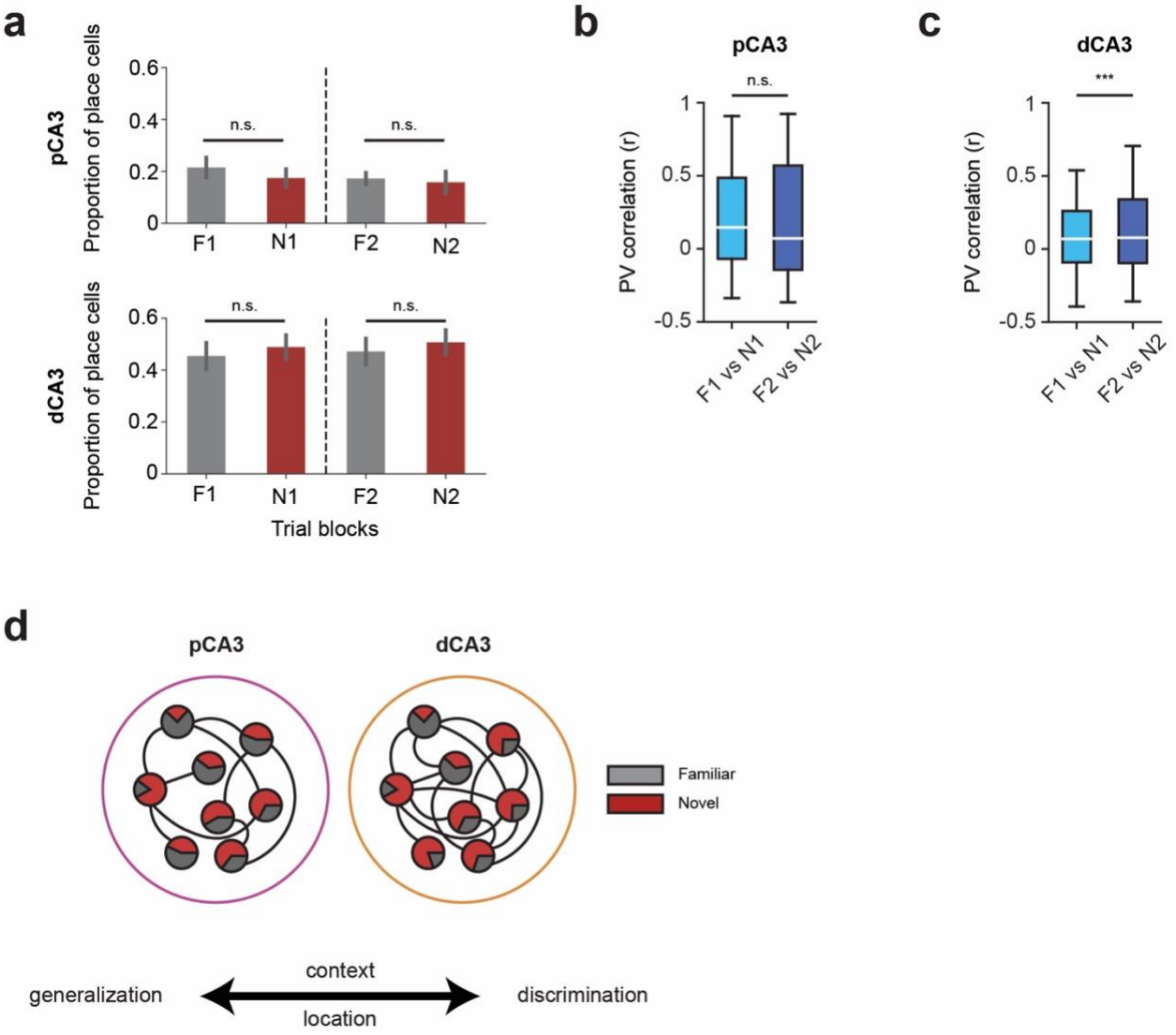

Supplementary Figure 4. (Related to Figure 2) **Place cell responses across blocks in a context-switching task. a.** Proportion of place cells in each trial block in pCA3 (top) and dCA3 (bottom). Familiar and novel blocks showed similar levels of place cells in both the first and second exposures (Kruskal-Wallis H-test, H = 1.43, p = 0.69 for pCA3, H = 0.73, p = 0.87 for dCA3). **c**-**d**. PV correlation between familiar and novel contexts for the first and second blocks. No significant difference was observed in pCA3 between the first and second blocks (p = 0.71), whereas a significant difference was found in dCA3 (p = 0.0003). **d**. Schematics showing gradients of generalization and discrimination of context and location by proximodistal CA3 with different levels of recurrent connection. Colors are matched as follows: purple for pCA3, orange for dCA3, gray for familiar context, and red for novel context. n.s. = non-significant, *p < 0.05, **p < 0.01, ***p < 0.001.

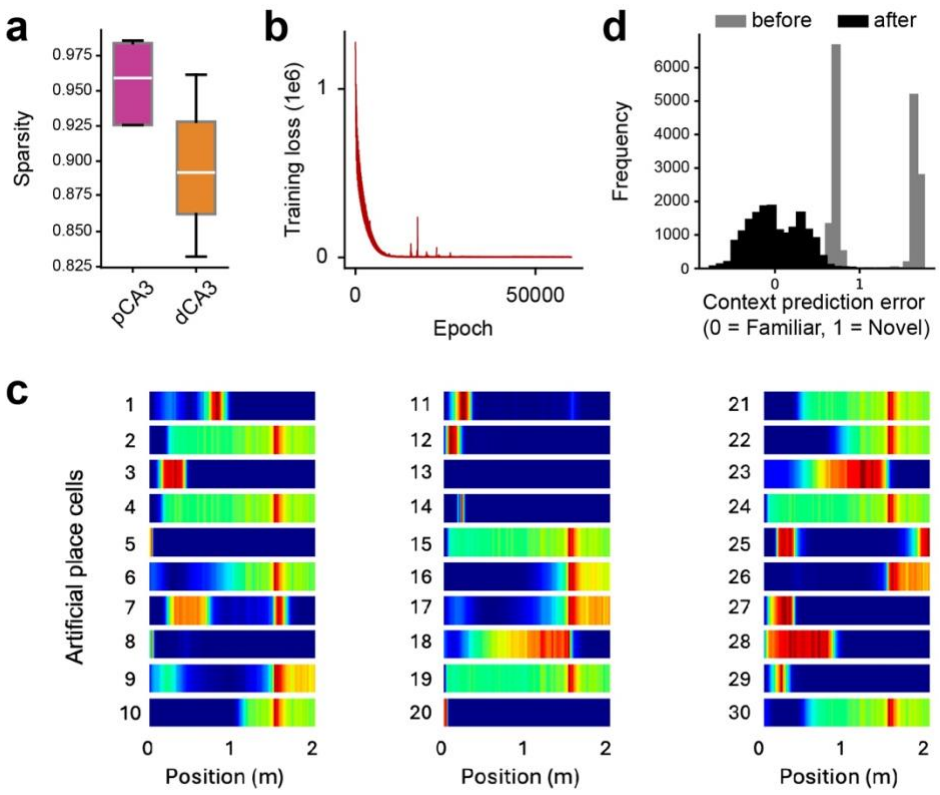

Supplementary Figure 5. (Related to Figure 3) **Spatial tuning properties of *in silico* place cells in RNN. a**. Comparing sparsity level via functional connectivity matrices: sparsity is evaluated based on the functional connectivity matrix of neurons in each subregion, using a 20-neuron window for both distal and proximal recordings. Results averaged across a recording session align with physiological studies, indicating greater recurrence in the dCA3 subregion. **b**. Training loss of multi-task RNN: the training loss curve for the multi-task RNN (referenced in Fig. 3f) demonstrates the stability of the model's convergence. **c**. spatial RNN tuning curve with different neuron number: Example of tuning curves for a spatial RNN network, modeled with varying neuron counts (30 neurons), highlighting the network's spatial encoding capabilities. **d**. Distribution of prediction error across all laps before (gray) and after (black) training RNN.

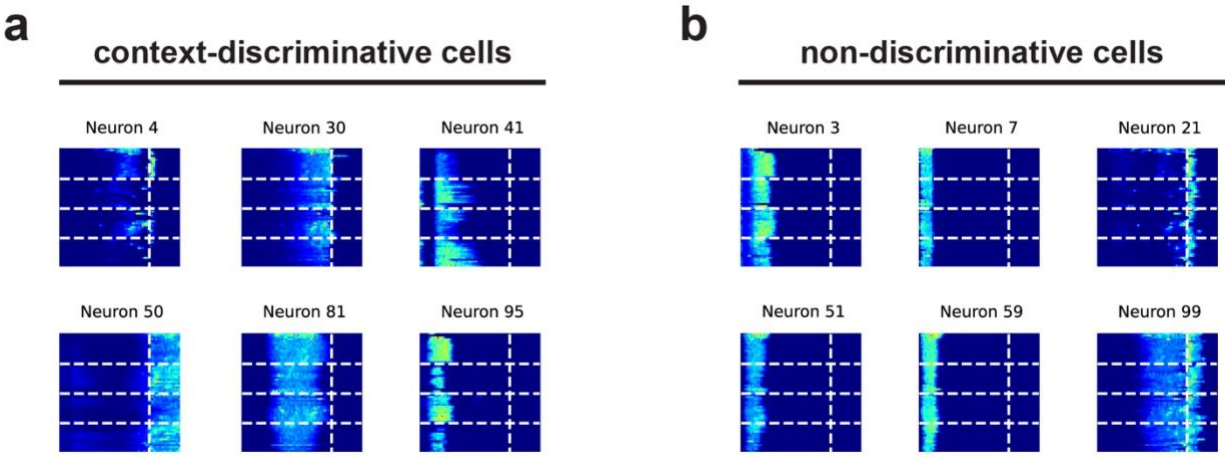

Supplementary Figure 6. (Related to Figure 3) **RNN artificial cell responses during context-switching task.** Example heatmaps of lap-by-lap activity for RNN artificial cells are shown. Context-discriminative cells (**a**) and non-discriminative cells (**b**). Horizonal dashed lines indicate context changes, and vertical dashed lines indicate the reward location.